Tuning the Electronic Structure of Bimetallic CoCu Clusters for Efficient Hydrolysis of Ammonia Borane

Yufeng Chen,[1#] Kang Wang,[1#] Kaiqi Nie,[2] Jiaou Wang,[2] Shifeng Wang,[3] Kun Feng[1]* and Jun Zhong[1]*

[1] *Institute of Functional Nano and Soft Materials Laboratory (FUNSOM), Jiangsu Key Laboratory for Carbon-Based Functional Materials & Devices, Soochow University, Suzhou 215123, China*

[2] *Institute of High Energy Physics, Chinese Academy of Sciences, Beijing 100049, China*

[3] *School of Energy and Electronic Engineering, University of Portsmouth, Portsmouth, UK*

[#] These authors contribute equally to this work.

* Corresponding authors: fengkun0520@163.com (Kun Feng), jzhong@suda.edu.cn (Jun Zhong)

Abstract: Efficient and low cost catalysts for the hydrogen production from ammonia borane (AB) are highly required to build up the upcoming hydrogen economy. Here we demonstrated that the non-active material could be directly transformed to highly active catalyst for the hydrolysis of AB when the surface parts were stripped to form tiny clusters on graphene oxide (GO), with the presence of strong cluster-support interaction. Moreover, the catalytic activity can be greatly enhanced by further tuning the electronic structure of clusters with various compositions. As a result, the final bimetallic CoCu catalyst on GO can achieve a high total turnover frequency (TOF) value of 72.4 (H_2) mol/(Cat-metal) mol·min with an activation energy of 47.8 kJ/mol, which is over 3 times higher than the monometallic clusters on GO. The cluster-support interaction has been clearly identified by synchrotron radiation X-ray absorption spectroscopy. An internal charge transfer from Cu to Co in the clusters can also be identified, which will weaken the B-N bond in AB and then effectively accelerate the hydrolysis of AB to achieve the high performance.

Keywords: ammonia borane, hydrolysis, X-ray absorption spectroscopy, clusters

1. Introduction

Developing clean and renewable energy sources to replace fossil fuels is important for our future life [1,2]. Among the most alternatives, hydrogen energy, owning to its various advantages, has been widely studied as a promising fuel [3,4]. To realize the hydrogen-based economics, controlled storage and transportation of hydrogen is of

great significance, while the chemical storage of hydrogen has been regarded as a viable pathway for this goal [1,2,5-7]. Recently, ammonia-borane (AB), as an outstanding material for chemical H_2 storage and production, has been considered as a promising candidate because of its high hydrogen content (19.6 wt%), high stability in aqueous solution and non-toxicity [7,8]. Noble metal-based catalysts typically show high efficiency for the hydrolysis of AB [9-14], however, the high cost and scarcity hamper their widespread applications. It is urgent to develop the alternate catalysts that based on inexpensive non-noble metal elements for highly efficient hydrolysis of AB.

Various transition metal elements such as Co, Ni, or Cu have been proved to be active for the hydrolysis of AB [8-10]. However, the corresponding catalytic activity is still unsatisfied when compared to the noble metal based catalysts [8-10]. To increase the catalytic activity, catalysts in the forms of single-atom catalysts (SACs) or tiny clusters have been proved to be very effective due to the fully exposed surface active sites [15-23]. Especially, tiny clusters not only showed superior catalytic activity in many energy-related applications, but also exhibited excellent tunability with the presence of various elements [15,16,24-28]. For example, Yu *et al.* reported the sub-nanometer bimetallic RhRu clusters for the hydrolysis of AB, which showed superior activity owning to the synergistic effect among Rh, Ru and the substrate [15]. Recently, the fully exposed palladium cluster catalysts even showed a better catalytic activity than the corresponding SACs [16]. Although tiny clusters have been widely reported to increase the performance, the detailed catalytic mechanism is still an open question.

The precise control of electronic structure in the catalysts, especially tuning the compositions in tiny clusters and creating the suitable interfacial interaction between clusters and substrate, remains a great challenge.

In this work, transition metal based tiny clusters can be directly stripped from the metal foam and then adhere on graphene oxide (GO) to form active catalysts. Interestingly, the same materials are originally inactive in the bulk foam, while they are highly active for the hydrolysis of AB when separated as tiny clusters on GO. Moreover, by tuning the compositions in bimetallic clusters (BCs), the catalytic activities can be greatly enhanced by at least 3 times. Thus by forming tiny clusters on GO and choosing the suitable elements, the non-active materials can be transformed to excellent catalysts for the hydrolysis of AB, fully demonstrating the advantage of tiny clusters as efficient catalysts. As a result, the final CoCu-BCs/GO catalyst shows a high total turnover frequency (TOF) value of 72.4 (H_2) mol/(Cat-metal) mol·min with an activation energy of 47.8 kJ/mol. The interfacial interaction between clusters and GO has been identified by using synchrotron radiation X-ray absorption spectroscopy (XAS). Moreover, XAS reveals the existence of internal charge transfer from Cu to Co in the clusters, which can weaken the B-N bond in AB and then effectively accelerate the hydrolysis of AB to achieve the high catalytic performance.

2. Experimental Materials

2.1. Chemical reagents

Chemical reagents were all analytical grade and directly used without purification. Sodium dodecyl sulfate (SDS, 95%), boric acid (99%), sodium borohydride (98%), sodium hydroxide (≥ 95%) and potassium permanganate (99%) were purchased from Sinopharm Chemical Reagent Co., Ltd. Cobalt sulfate heptahydrate (99%) and graphite (< 20 μm) were purchased from Aladdin. Hydrochloric acid (36 ~ 38%), ethanol absolute (GR), hydrogen peroxide (30%) and sulfuric acid (95 ~ 98%) were purchased from Yonghua Chemical Co., Ltd. Ammonia borane (AB, 97%) was purchased from Sigma-Aldrich. De-ionized water was obtained from an ultra-pure purifier (resistivity ≥ 18.2 MΩ).

2.2. Synthesis of CoCu foam

Co foam, Ni foam and Cu foam were commercially obtained and washed by acetone, ethanol, 5% HCl and distilled water in sequence via ultrasonic bath to remove contaminations and surface oxide layer. CoCu foam was prepared by an electrodeposition method, which was conducted in a conventional three-electrode setup (CHI-760E, Shanghai) with clean Cu foam as the working electrode, Co plate as the counter electrode, and Ag/AgCl as the reference electrode. Cu foam was immersed in the electrolyte containing 0.18 M $CoSO_4 \cdot 7H_2O$, 0.8 M H_3BO_3 and 2 mM SDS, with an applied potential of -1.5 V (vs. Ag/AgCl) for 30 min. The obtained CoCu foam was washed with distilled water and ethanol and then dried under room temperature. Finally, it was heated in a tube furnace at 950 °C for 2 h under 5% H_2/Ar atmosphere to remove the surface oxidation layer. CoNi foam was prepared through the same process except

for using Ni foam instead of Cu foam. Pure metal foams (Co foam, Ni foam and Cu foam) were also treated at 950 °C under 5% H_2/Ar atmosphere to remove the oxidation layer for further modification.

2.3. Synthesis of CoCu/GO

GO was prepared from natural graphite by a modified Hummers' method. CoCu foam was immersed in the GO ethanol solution (6 mg/mL) for about 5 seconds. Then the foam was dried in vacuum at 25 ^{o}C for 24 h. The CoCu foam with GO was soaked in 50 mL ethanol solution with sonication for 1 h. Then CoCu clusters could be directly stripped to form the CoCu/GO in solution. The obtained solution was filtrated and washed. The product was cooled and freeze-dried overnight to obtain the CoCu/GO powder (CoCu-BCs/GO). The control samples (CoNi-BCs/GO, Co-Cs/GO, Ni-Cs/GO and Cu-Cs/GO) were prepared through the similar process except for changing the corresponding metal foams.

2.4. Structural characterization

The morphology was characterized by high-resolution transmission electron microscope (HRTEM) (FEI Talos F200X), Aberration-corrected high-angle annular dark-field scanning transmission electron microscope (FEI Titan Themis G2) and Scanning electron microscope (Zeiss G500). X-ray photoelectron spectrometer (XPS, Kratos AXIS UltraDLD) and X-ray diffraction (XRD, PANalytical B.V. Empyrean powder diffractometer equipped with PIXcel3D detector) were also used. The elemental contents were obtained from an inductively coupled plasma (ICP)

spectrometer (VISTA-MPX (CCD Simultaneous ICP-OES), Varian). X-ray absorption spectroscopy (XAS) experiments were performed at the National Synchrotron Radiation Laboratory (NSRL, Beamlines MCD-A and MCD-B (Soochow Beamline for Energy Materials)), Beijing Synchrotron Radiation Facility (BSRF, 4B9B) and the Shanghai Synchrotron Radiation Facility (SSRF, 11B). The EXAFS data was treated by Athena software.

2.5. Catalytic Activity Measurement

A one-neck round-bottom flask (25 mL) sealed and connected to a gas collecting tube was used for the hydrolysis of AB. Typically, 5 mg catalyst powder and 2 mL aqueous solution with 0.5 M NaOH were filled in the flask with stirring for a few min at room temperature. Then, 1 mL NaOH (0.5 M) aqueous solution containing 15.4 mg AB (0.5 mmol) was quickly injected into the flask. The experiment was performed under room temperature and ambient atmosphere. The reaction time was recorded when observing the first bubble (after AB injection there is about 5 s to observe the first bubble). The volume of hydrogen generation was measured by recording the displacement of water. The product gas was identified using a gas chromatograph (GC7890T system, using N_2 as carrier gas). The hydrolysis process can be described by the formula: $NH_3BH_3 + 2H_2O = NH_4^+ + BO_2^- + 3H_2$. TOF numbers are calculated by the formula: TOF = $\frac{n_{H2}}{n_{metal} \times t}$. In which n_{H2} is the mole number of generated H_2, while n_{metal} is the total mole number of metal (Cu and Co), t is the completed reaction time (min). The hydrolysis reaction was repeated for 5 times to measure the stability.

The activation energy was calculated by Arrhenius equation: $\ln k = \frac{-E_a}{RT} + C$. In which k is reaction rate, E_a is activation energy, T is reaction temperature, R is molar gas constant, C is a constant. The catalytic activity was also measured at 328 K, 318 K, 308 K and 298 K, respectively.

3. Results and Discussion

3.1. Morphology and Structure Characterization

As illustrated in Fig. 1a, GO can firstly adhere on the metal foam through interfacial interaction (for example, bonding between metal and oxygen-containing groups on GO). Then under sonication, CoCu bimetallic clusters can be stripped from the metal foam and form the hybrid of CoCu bimetallic clusters on GO (denoted as CoCu-BCs/GO). Various tiny clusters on GO can also be prepared by using the same method [29]. Detailed synthesis information can be found in the Experimental section. Transmission electron microscope (TEM) image of the CoCu-BCs/GO catalyst is shown in Fig. 1b, while no obvious metal particles on GO can be observed due to the small cluster size. TEM image of CoCu-BCs/GO in Fig. S1a also shows no clear particles. However, the dark field elemental mappings of CoCu-BCs/GO in Fig. 1c strongly confirm the existence of Co and Cu on GO. In order to clearly reveal the existence of CoCu clusters on GO, aberration-corrected high-angle annular dark-field scanning transmission electron microscopy (HAADF-STEM) was used and the results were shown in Fig. 1d. It is clear that large amounts of clusters less than 1 nm can be observed on the GO support (labeled by red circles), confirming the existence of metal based clusters. X-ray

diffraction (XRD) spectra of pure GO and CoCu-BCs/GO are also shown in Fig. S1b. Both the sharp peak at around 10º and the broad peak at around 20º can be attributed to the characteristic peaks of GO [30], while no new peaks can be observed for CoCu clusters due to the ultra-small size [31,32]. Fig. S2 also shows the TEM image and elemental mappings of pure GO. The metal contents in the CoCu-BCs/GO catalyst are shown Table S1 (measured by ICP-OES), with a value of 1.91 wt% for Cu and a value of 3.01 wt% for Co. The metal contents have been optimized by changing the electrodeposition time to achieve the best performance. For comparison, various monometallic clusters (M-Cs) on GO (denoted as Co-Cs/GO, Ni-Cs/GO and Cu-Cs/GO) are also prepared with the TEM images shown in Fig. S3 and the metal contents shown in Table S1.

X-ray photoelectron spectroscopy (XPS) spectra at Cu and Co 2*p* have been measured to probe the chemical states and the results are shown in Fig. S4. The Cu 2*p* spectra of both CoCu-BCs/GO and reference Co-Cs/GO in Fig. S4b show two prominent peaks at around 932.1 and 952 eV, which can be assigned to Cu^{2+} $2p_{3/2}$ and $2p_{1/2}$ [33,34], respectively, suggesting the oxidized Cu state on GO. Two strong satellite peaks at around 940 and 960 eV also confirm the oxidized state of Cu^{2+} similar to CuO [33,34]. It is consistent with the preparation process that through the interfacial C-O-M bonds (GO and metal), metal based clusters can be stripped from the metal foam. Small metallic clusters can also be easily oxidized in air. The Co 2*p* spectra in Fig. 4a also show two main peaks (781.2 and 797.2 eV for Co $2p_{3/2}$ and $2p_{1/2}$, respectively) and two

satellite peaks (785.8 and 802.7 eV), standing for the existence of CoO [35-37].

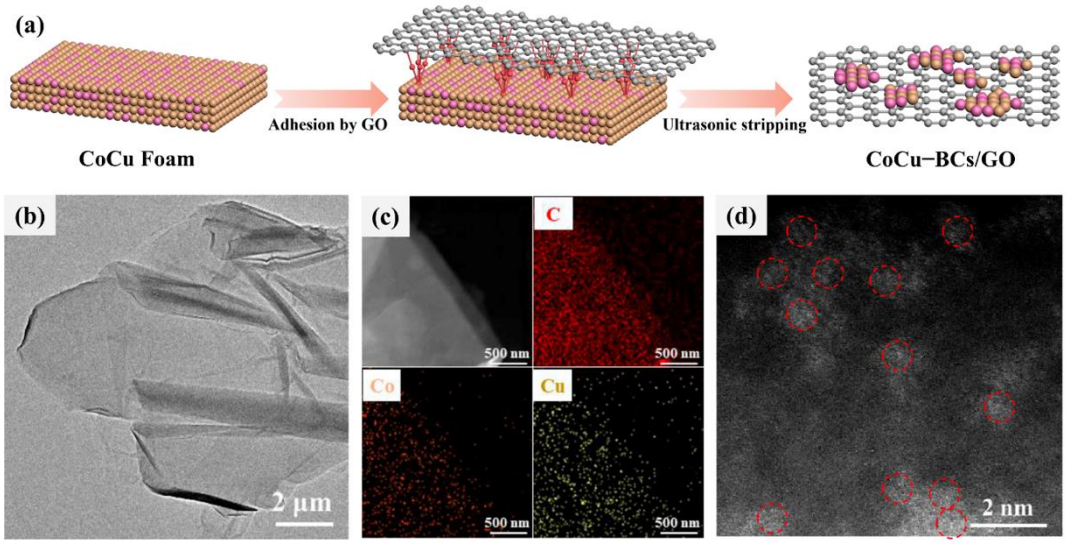

Fig. 1. Illustration and TEM images of CoCu-BCs/GO. (**a**) The preparation process of CoCu-BCs/GO. (**b**) TEM image, (**c**) dark field elemental mappings of CoCu-BCs/GO: C (red), Co (orange) and Cu (yellow). (**d**) Aberration-corrected HAADF-STEM image of CoCu-BCs/GO.

To clearly understand the electronic structure of CoCu-BCs/GO, synchrotron radiation XAS experiments in hard X-ray range have been performed. Fig. 2a shows the normalized X-ray Absorption Near Edge Structure (XANES) spectra at Co *K*-edge. The spectrum of CoCu-BCs/GO shows a pre-edge peak A at around 7710 eV and a strong white line peak B at around 7725 eV, similar to that of CoO. The corresponding Extended X-ray Absorption Fine Structure (EXAFS) data of CoCu-BCs/GO is shown in Fig. 2b, which exhibits a main peak at 1.58 Å for the Co-O bond. Interestingly, no Co-Co coordination as that in CoO or Co foil can be observed (labeled by red ellipse) in CoCu-BCs/GO, suggesting the ultra-small size of Co-based clusters in CoCu-

BCs/GO (like SACs) [38,39]. The XANES spectrum of CoCu-BCs/GO at Cu *K*-edge is also shown in Fig. 2c, which is similar to that of CuO. The corresponding EXAFS data in Fig. 2d also shows the presence of Cu-O bonds while no Cu-Cu coordination as that in CuO or Cu foil can be observed. The XANES results clearly reveal that both Co and Cu in CoCu-BCs/GO have been oxidized, while the EXAFS data strongly confirm the existence of tiny clusters on GO in good agreement with the HAADF-STEM results. The clusters in CoCu-BCs/GO should be CoCuO with Co-O-Cu geometry instead of metallic Cu-Co alloy.

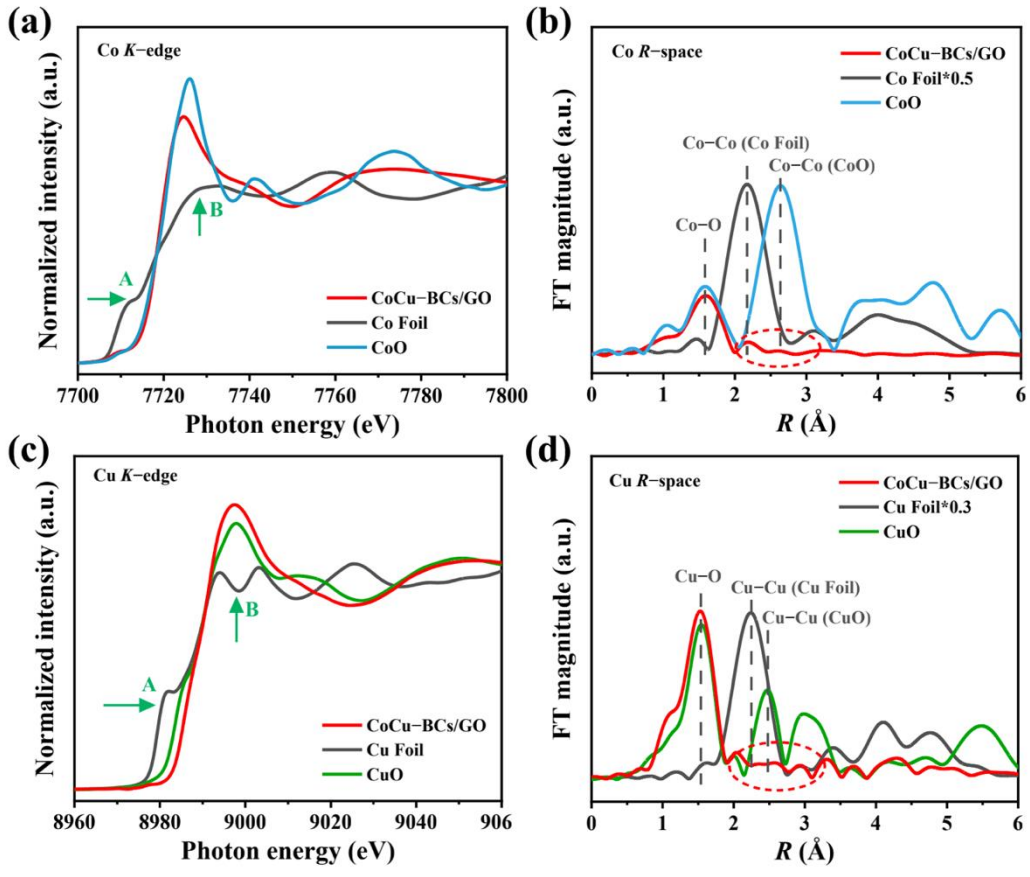

Fig. 2. Structure identification of CoCu-BCs/GO. (**a**) Normalized XANES spectra of CoCu-BCs/GO, Co foil, and CoO at Co *K*-edge. (**c**) Normalized XANES spectra of

CoCu-BCs/GO, Cu Foil, and CuO at Cu *K*-edge. **(b)** and **(d)** Corresponding k^3-weighted Fourier transform curves of the EXAFS data.

More evidence for the presence of tiny CoCu bimetallic clusters on GO can be found in the wavelet transform (WT) plots at Co and Cu *K*-edges, as shown in Fig. S5. WT plots are widely known to simultaneously show the *k* and *R* space data. For CoCu-BCs/GO, the strongest peak at Co *K*-edge (Fig. S5c) exists at *k* value of ~ 5.61 $Å^{-1}$ and *R* value of ~ 1.58 Å for Co-O bonds. For comparison, the peaks at higher *k* and *R* values for Co-Co in CoO and Co Foil cannot be observed in the WT plot of CoCu-BCs/GO, confirming the ultra-small size of clusters. The WT plot of CoCu-BCs/GO at Cu *K*-edge also shows similar results in Fig. S5f. The fitting curves of EXAFS data at Cu and Co *K*-edges are shown in Fig. S6 and the results can be found in Table S2, suggesting the oxidized Cu and Co environment in CoCu-BCs/GO.

3.2. Catalytic performance

The catalytic activities of various catalysts for the hydrolysis of AB have been evaluated under room temperature and ambient atmosphere. Details of the measurement can be found in the experimental section. Pure GO shows no catalytic activity for the hydrolysis of AB (Fig. S7a). The catalytic properties of various metal foams (Co foam, Ni foam, Cu foam) are also shown in Fig. 3a, while all the three foams exhibit almost no activity in a long reaction time. Interestingly, when the same surface materials have

been stripped from the metal foam to form tiny clusters on GO with a strong interfacial interaction, all the obtained catalysts (Co-Cs/GO, Ni-Cs/GO, and Cu-Cs/GO) are active for the hydrolysis of AB. Especially, the Co-Cs/GO catalyst shows a good TOF value of 23.9 (H_2) mol/(Cat-metal) mol·min (Fig. 3b and 3c). The results clearly demonstrate that by decreasing the material size to tiny clusters, materials which are initially non-active can be transformed to good catalysts along with the assistance of a suitable substrate like GO. The creation of tiny clusters can thus be an effective way to build up efficient catalysts for various applications.

Moreover, the activity can be further tuned by controlling the metal elements in the tiny clusters. Fig. 3b shows the catalytic activities of bimetallic foams (CoCu and CoNi foams). Similar to monometallic foams, both CoCu and CoNi foams show almost no catalytic activity for the hydrolysis of AB. However, when the CoCu and CoNi clusters have been stripped from the metal foams to form the hybrids of bimetallic clusters on GO, their hydrolysis activities can be greatly enhanced. Especially, the CoCu-BCs/GO sample can reach an excellent TOF value up to 72.4 (H_2) mol/(Cat-metal) mol·min, which is around 3.0 or 4.6 times to that of monometallic Co-Cs/GO or Cu-Cs/GO catalysts, respectively. The hydrogen evolution reaction can be finished in 5 min by using the CoCu-BCs/GO catalysts as shown in Fig. 3b, while it needs more than 20 min to release all the hydrogen by using Co-Cs/GO or Cu-Cs/GO. The enhanced performance can be attributed to the synergistic effect between Co and Cu by tuning the electronic structure to a favorable state for the hydrolysis reaction. This method can

also be extended to various metal elements. For example, the combination of Co and Ni in clusters also exhibits significantly enhanced performance by forming the CoNi-BCs/GO hybrid (TOF is 33.6 compared to 23.9 and 6.8 for Co-Cs/GO and Ni-Cs/GO, respectively), as shown in Fig. 3b and 3c. The high catalytic activity of CoCu-BCs/GO for the hydrolysis of AB is also compared with the values reported in the literature as shown in Table S3, which is a good value for non-noble metal element based catalysts. The stability curves of CoCu-BCs/GO are also shown in Fig. 3d, which show no obvious activity decay in 5 cycles (60% left). Fig. S8a shows the catalytic activity curves of CoCu-BCs/GO at different temperature and Fig. S8b shows the corresponding Arrhenius plot, which can be used to calculate the activation energy [30,40]. The obtained activation energy is 47.8 kJ/mol for CoCu-BCs/GO, in good agreement with the high catalytic activity [8,40].

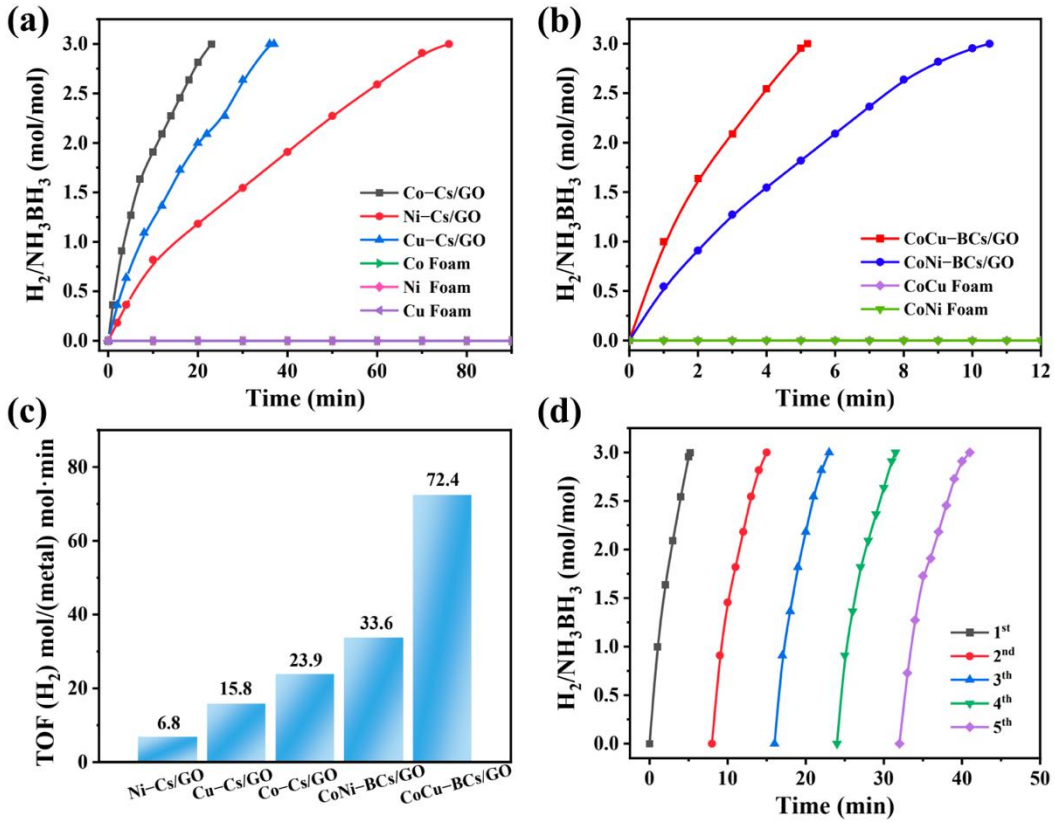

Fig. 3. Catalytic performance of various catalysts for the hydrolysis of AB. (a) Hydrogen evolution curves catalyzed by various monometallic clusters on GO (Co-Cs/GO, Ni-Cs/GO, and Cu-Cs/GO) and monometallic foams (Co, Ni, and Cu foams). (b) Hydrogen evolution curves catalyzed by bimetallic clusters on GO (CoCu-BCs/GO and CoNi-BCs/GO) and bimetallic foams (CoCu and CoNi foams). (c) The TOF values of various catalysts. (d) Stability test of CoCu-BCs/GO in 5 cycles.

3.3. Working Mechanism

XAS spectra of GO and CoCu-BCs/GO at C *K*-edge are compared in Fig. S9, which can be used to reveal the interfacial interaction between the active clusters and the GO support. Both spectra show three typical features labeled as A, B and D at about 285.5, 288.9 and 293.1 eV, respectively, which are in line with the typical GO structure [30,41].

Features A and D can be assigned to the transitions from C 1s to the unoccupied π* and σ* orbitals, respectively, confirming the carbon ring structure of GO in both samples. Feature B can be attributed to the interaction between carbon and other elements [30,41]. For pure GO, a prominent feature B can be observed standing for the presence of abundant C-O groups (COOH, C=O, or C-OH). When coupling with the metal based clusters, the XAS spectrum of CoCu-BCs/GO shows an enhanced feature B, which can be attributed to the strong interfacial interaction between GO substrate and CoCu bimetallic clusters [30]. The interfacial interaction can both anchor the clusters on GO and accelerate the charge transfer between GO and clusters, then facilitate the hydrolysis reaction.

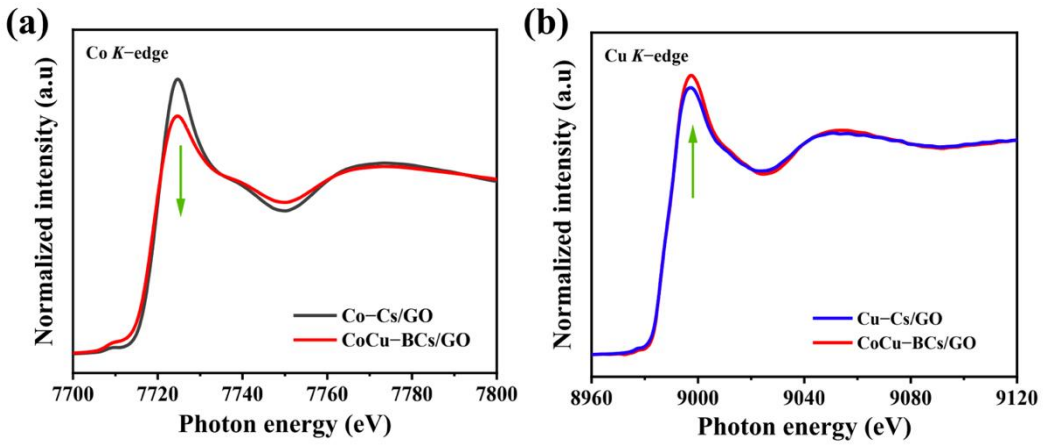

Fig. 4. Structure comparison between bimetallic and monometallic clusters. (**a**) Normalized XANES spectra of CoCu-BCs/GO and Co-Cs/GO at Co *K*-edge. (**b**) Normalized XANES spectra of CoCu-BCs/GO and Cu-Cs/GO at Cu *K*-edge.

To further understand the electronic structure of CoCu-BCs/GO for the enhanced hydrolysis of AB, the XANES spectra of bimetallic clusters and monometallic clusters

296 on GO are compared in Fig. 4. The corresponding EXAFS curves of monometallic
297 clusters on GO (Co-Cs/GO and Cu-Cs/GO) can also be found in Fig. S10. Similar to
298 the bimetallic CoCu sample (Fig. 2), both Co-Cs/GO and Cu-Cs/GO in Fig. S10 show
299 very weak metal-metal (Co-Co or Cu-Cu) coordination in the EXAFS spectra,
300 confirming the ultra-small size of metal-based clusters in Co-Cs/GO and Cu-Cs/GO
301 [38,39]. The main peaks in Fig. S10 can also be attributed to Co-O or Cu-O for Co-
302 Cs/GO or Cu-Cs/GO, respectively. Interestingly, when the two metal elements have
303 been coupled in CoCu-BCs/GO, different capabilities to gain electrons of the two
304 elements can be observed. As shown in Fig. 4a, the XANES spectrum of CoCu-BCs/GO
305 shows an obviously decreased intensity of the white line peak when compared to that
306 of Co-Cs/GO at Co *K*-edge, suggesting more electrons obtained to fill the unoccupied
307 states of Co with the presence of Cu. As a comparison, the Cu *K*-edge XANES spectrum
308 of CoCu-BCs/GO in Fig. 4b shows an increased white line peak intensity, standing for
309 the loss of electrons at the Cu sites due to the presence of Co. The slight energy shifts
310 at the Cu (positive shift) and Co (negative shift) *L*-edges in Fig. S11 also confirm the
311 charge transfer from Cu to Co. Thus a charge re-arrangement can occur in the bimetallic
312 clusters with the electrons transferred from Cu to Co, leading to a favorable chemical
313 state to weaken the B-N bond in AB for the accelerated hydrolysis reaction [30,37]. Our
314 previous work showed that the Co-O-Cu geometry in oxidized Cu-Co compounds had
315 a Co-Cu distance similar to that between the H atom bound to B atoms and the H atom
316 bound to N atoms in AB (2.68 Å) [37]. With the favorable geometry and different

capabilities to gain electrons on the two elemental sites, the catalyst can thus anchor the AB molecules and be favorable for the weakening of B-N bonds. Since the synthesis methods for both bimetallic clusters and monometallic clusters on GO are very similar, the cluster size and the interaction between clusters and Go are also similar, then the obviously different electronic structures in bimetallic clusters and monometallic clusters may play a key role for the enhanced performance. As a result, the hydrolysis activity can be greatly improved from 23.9 (for Co-Cs/GO) or 15.8 (Cu-Cs/GO) to 72.4 (CoCu-BCs/GO) (H_2) mol/(Cat-metal) mol·min (Fig. 3c). Tuning the electronic structure in tiny clusters by using various elements, along with the strong interfacial catalyst-support interaction, can thus be a very effective way to improve the catalytic activity. Actually, the hydrogen evolution curve catalyzed by the physical mixture of Co-Cs/GO and Cu-Cs/GO is also compared in Fig. S7b, while the corresponding catalytic performance is much lower than that of the CoCu-BCs/GO catalyst due to the lack of interaction between Co and Cu. Fig. S7c also compares the hydrogen evolution curves in 0.5 M NaOH and in neutral water (TOF value is 41.8), revealing that the alkaline environment is favorable for the hydrolysis reaction.

The working mechanism can thus be illustrated according to the above discussion. A strong interfacial interaction can be found between GO and the metal oxide clusters, which can both anchor the clusters on GO and accelerate the charge transfer between GO and clusters for better performance. The clusters can thus be activated for the hydrolysis of AB, and can be oxidized when exposed to air. Moreover, the catalytic

performance can be further enhanced by forming bimetallic compounds. The Co-O-Cu geometry in oxidized clusters can help to anchor AB molecules in the reaction. A charge re-arrangement can also occur in the bimetallic clusters with an electron transfer from Cu to Co, which is favorable to further anchor AB and then weaken the B-N bonds for enhanced performance.

4. Conclusions

In conclusion, this work reports the bimetallic CoCu clusters anchored on GO for the efficient hydrolysis of AB. By forming the tiny clusters on GO, the initially non-active metal can be transformed to highly active catalyst for the hydrolysis of AB. XAS has been used to reveal the existence of interfacial interaction between clusters and GO. Moreover, the catalytic activity can be further enhanced by tuning the electronic structure of clusters with various elements such as Co and Cu. An internal charge transfer from Cu to Co in the clusters can be identified, which may weaken the B-N bond in AB and then effectively accelerate the hydrolysis reaction. Owning to the favorable design of bimetallic CoCu clusters supported on GO, the CoCu-BCs/GO catalyst shows a high TOF value of 72.4 (H_2) mol/(Cat-metal) mol·min with an activation energy of 47.8 kJ/mol. The design with fully exposed bimetallic clusters on suitable support may offer a new way for the rational design of highly efficient catalysts to produce hydrogen.

Declaration of competing interest

The authors declare no competing financial interests.

Acknowledgments

We acknowledge the support from NSRL (MCD-A and MCD-B, Soochow Beamline for Energy Materials), BSRF (4B9B), and SSRF (11B) for the XAS experiments. This work is supported by the National Key R&D Program of China (2020YFA0406103), the National Natural Science Foundation of China (U1932211), the Collaborative Innovation Center of Suzhou Nano Science & Technology, the Priority Academic Program Development of Jiangsu Higher Education Institutions (PAPD), and the 111 Project.

Appendix A. Supplementary data

Additional TEM images, XPS analyses, XAS spectra, electrochemical measurements and three tables. The Supporting Information is available free of charge in the online version of this article.

References

[1] S. Chu, Y. Cui, N. Liu, The path towards sustainable energy, Nat. Mater. 16 (2016) 16-22.

[2] S. Chu, A. Majumdar, Opportunities and challenges for a sustainable energy future, Nature 488 (2012) 294-303.

[3] J. Zhu, L. Hu, P. Zhao, L.Y.S. Lee, K.-Y. Wong, Recent Advances in Electrocatalytic Hydrogen Evolution Using Nanoparticles, Chem. Rev. 120 (2020) 851-918.

[4] A.J. Shih, S.M. Haile, Electrifying membranes to deliver hydrogen, Science 376

(2022) 348-349.

[5] T. He, P. Pachfule, H. Wu, Q. Xu, P. Chen, Hydrogen carriers, Nat. Rev. Mater. 1 (2016) 16059.

[6] S. Liu, J. Liu, X. Liu, J. Shang, L. Xu, R. Yu, J. Shui, Hydrogen storage in incompletely etched multilayer Ti_2CT_x at room temperature, Nat. Nanotechnol. 16 (2021) 331-336.

[7] Q. Sun, N. Wang, T. Zhang, R. Bai, A. Mayoral, P. Zhang, Q. Zhang, O. Terasaki, J. Yu, Zeolite-Encaged Single-Atom Rhodium Catalysts: Highly-Efficient Hydrogen Generation and Shape-Selective Tandem Hydrogenation of Nitroarenes, Angew. Chem. Int. Ed. 58 (2019) 18570-18576.

[8] Y. Chen, K. Feng, G. Yuan, Z. Kang, J. Zhong, Highly efficient CoNiP nanoboxes on graphene oxide for the hydrolysis of ammonia borane, Chem. Eng. J. 428 (2022) 131219.

[9] J. Zhang, X. Zheng, W. Yu, X. Feng, Y. Qin, Unravelling the synergy in platinum-nickel bimetal catalysts designed by atomic layer deposition for efficient hydrolytic dehydrogenation of ammonia borane, Appl. Catal. B-Environ. 306 (2022) 121116.

[10] X. Huang, Y. Liu, H. Wen, R. Shen, S. Mehdi, X. Wu, E. Liang, X. Guo, B. Li, Ensemble-boosting effect of Ru-Cu alloy on catalytic activity towards hydrogen evolution in ammonia borane hydrolysis, Appl. Catal. B-Environ. 287 (2021) 119960.

[11] S. Zhou, Y. Yang, P. Yin, Z. Ren, L. Wang, M. Wei, Metal-Support Synergistic Catalysis in Pt/MoO_{3-x} Nanorods toward Ammonia Borane Hydrolysis with Efficient Hydrogen Generation, ACS Appl. Mater. Interfaces 14 (2022) 5275-5286.

[12] J. Li, Q. Guan, H. Wu, W. Liu, Y. Lin, Z. Sun, X. Ye, X. Zheng, H. Pan, J. Zhu, S. Chen, W. Zhang, S. Wei, J. Lu, Highly Active and Stable Metal Single-Atom Catalysts Achieved by Strong Electronic Metal-Support Interactions, J. Am.

Chem. Soc. 141 (2019) 14515-14519.

[13] H. Yan, Y. Lin, H. Wu, W. Zhang, Z. Sun, H. Cheng, W. Liu, C. Wang, J. Li, X. Huang, T. Yao, J. Yang, S. Wei, J. Lu, Bottom-up precise synthesis of stable platinum dimers on graphene, Nat. Commun. 8 (2017) 1070.

[14] Z. Li, T. He, D. Matsumura, S. Miao, A. Wu, L. Liu, G. Wu, P. Chen, Atomically Dispersed Pt on the Surface of Ni Particles: Synthesis and Catalytic Function in Hydrogen Generation from Aqueous Ammonia-Borane, ACS Catal. 7 (2017) 6762-6769.

[15] N. Wang, Q. Sun, T. Zhang, A. Mayoral, L. Li, X. Zhou, J. Xu, P. Zhang, J. Yu, Impregnating Subnanometer Metallic Nanocatalysts into Self-Pillared Zeolite Nanosheets, J. Am. Chem. Soc. 143 (2021) 6905-6914.

[16] C. Dong, Z. Gao, Y. Li, M. Peng, M. Wang, Y. Xu, C. Li, M. Xu, Y. Deng, X. Qin, F. Huang, X. Wei, Y.-G. Wang, H. Liu, W. Zhou, D. Ma, Fully exposed palladium cluster catalysts enable hydrogen production from nitrogen heterocycles, Nat. Catal. 5 (2022) 485-493.

[17] H. Jeong, O. Kwon, B.-S. Kim, J. Bae, S. Shin, H.-E. Kim, J. Kim, H. Lee, Highly durable metal ensemble catalysts with full dispersion for automotive applications beyond single-atom catalysts, Nat. Catal. 3 (2020) 368-375.

[18] X. Wang, L. Zhao, X. Li, Y. Liu, Y. Wang, Q. Yao, J. Xie, Q. Xue, Z. Yan, X. Yuan, W. Xing, Atomic-precision Pt_6 nanoclusters for enhanced hydrogen electro-oxidation, Nat. Commun. 13 (2022) 1596.

[19] Y. Ge, X. Qin, A. Li, Y. Deng, L. Lin, M. Zhang, Q. Yu, S. Li, M. Peng, Y. Xu, X. Zhao, M. Xu, W. Zhou, S. Yao, D. Ma, Maximizing the Synergistic Effect of CoNi Catalyst on α-MoC for Robust Hydrogen Production, J. Am. Chem. Soc. 143 (2021) 628-633.

[20] P.-C. Poon, Y. Wang, W. Li, D.W.-S. Suen, W.W.Y. Lam, D.Z.J. Yap, B.L. Mehdi, J. Qi, X.-Y. Lu, E.Y.C. Wong, C. Yang, C.-W. Tsang, Synergistic effect of Co catalysts with atomically dispersed CoN_x active sites on ammonia borane

hydrolysis for hydrogen generation, J. Mater. Chem. A 10 (2022) 5580-5592.

[21] L. Chen, Z. Qi, S. Zhang, J. Su, G.A. Somorjai, Application of Single-Site Catalysts in the Hydrogen Economy, Trends Chem. 2 (2020) 1114-1125.

[22] L. Wang, H. Li, W. Zhang, X. Zhao, J. Qiu, A. Li, X. Zheng, Z. Hu, R. Si, J. Zeng, Supported Rhodium Catalysts for Ammonia-Borane Hydrolysis: Dependence of the Catalytic Activity on the Highest Occupied State of the Single Rhodium Atoms, Angew. Chem. Int. Ed. 56 (2017) 4712-4718.

[23] S. Ji, B. Jiang, H. Hao, Y. Chen, J. Dong, Y. Mao, Z. Zhang, R. Gao, W. Chen, R. Zhang, Q. Liang, H. Li, S. Liu, Y. Wang, Q. Zhang, L. Gu, D. Duan, M. Liang, D. Wang, X. Yan, Y. Li, Matching the kinetics of natural enzymes with a single-atom iron nanozyme, Nat. Catal. 4 (2021) 407-417.

[24] M. Peng, C. Dong, R. Gao, D. Xiao, H. Liu, D. Ma, Fully Exposed Cluster Catalyst (FECC): Toward Rich Surface Sites and Full Atom Utilization Efficiency, ACS Cent. Sci. 7 (2021) 262-273.

[25] H. Jeong, G. Lee, B.S. Kim, J. Bae, J.W. Han, H. Lee, Fully Dispersed Rh Ensemble Catalyst To Enhance Low-Temperature Activity, J. Am. Chem. Soc. 140 (2018) 9558-9565.

[26] Q. Sun, N. Wang, R. Bai, Y. Hui, T. Zhang, D.A. Do, P. Zhang, L. Song, S. Miao, J. Yu, Synergetic Effect of Ultrasmall Metal Clusters and Zeolites Promoting Hydrogen Generation, Adv. Sci. 6 (2019) 1802350.

[27] H. Wu, X. Yang, S. Zhao, L. Zhai, G. Wang, B. Zhang, Y. Qin, Encapsulation of atomically dispersed Pt clusters in porous TiO_2 for semi-hydrogenation of phenylacetylene, Chem. Commun. 58 (2022) 1191-1194.

[28] W. Chen, W. Fu, G. Qian, B. Zhang, Chen, X. Duan, X. Zhou, Synergistic Pt-WO_3 Dual Active Sites to Boost Hydrogen Production from Ammonia Borane, iScience 23 (2020) 100922.

[29] Y. Qu, L. Wang, Z. Li, P. Li, Q. Zhang, Y. Lin, F. Zhou, H. Wang, Z. Yang, Y. Hu, M. Zhu, X. Zhao, X. Han, C. Wang, Q. Xu, L. Gu, J. Luo, L. Zheng, Y. Wu,

Ambient Synthesis of Single-Atom Catalysts from Bulk Metal via Trapping of Atoms by Surface Dangling Bonds, Adv. Mater. 31 (2019) 1904496.

[30] K. Feng, J. Zhong, B. Zhao, H. Zhang, L. Xu, X. Sun, S.T. Lee, $Cu_xCo_{1-x}O$ Nanoparticles on Graphene Oxide as A Synergistic Catalyst for High-Efficiency Hydrolysis of Ammonia-Borane, Angew. Chem. Int. Ed. 55 (2016) 11950-11954.

[31] Q.-L. Zhu, J. Li, Q. Xu, Immobilizing Metal Nanoparticles to Metal–Organic Frameworks with Size and Location Control for Optimizing Catalytic Performance, J. Am. Chem. Soc. 135 (2013) 10210-10213.

[32] H. Xu, B. Fei, G. Cai, Y. Ha, J. Liu, H. Jia, J. Zhang, M. Liu, R. Wu, Boronization-Induced Ultrathin 2D Nanosheets with Abundant Crystalline–Amorphous Phase Boundary Supported on Nickel Foam toward Efficient Water Splitting, Adv. Energy Mater. 10 (2020) 1902714.

[33] T. Soe, A. Jityen, T. Kongkaew, K. Subannajui, A. Sinsarp, T. Osotchan, X-ray photoelectron spectroscopy study of chromium and magnesium doped copper ferrite thin film, AIP Conference Proceedings 2279 (2020) 140002.

[34] M.C. Biesinger, L.W.M. Lau, A.R. Gerson, R.S.C. Smart, Resolving surface chemical states in XPS analysis of first row transition metals, oxides and hydroxides: Sc, Ti, V, Cu and Zn, Appl. Surf. Sci. 257 (2010) 887-898.

[35] M. Pang, G. Long, S. Jiang, Y. Ji, W. Han, B. Wang, X. Liu, Y. Xi, D. Wang, F. Xu, Ethanol-assisted solvothermal synthesis of porous nanostructured cobalt oxides (CoO/Co_3O_4) for high-performance supercapacitors, Chem. Eng. J. 280 (2015) 377-384.

[36] H. Woo, E. Kim, J.H. Kim, S.W. Yun, J.C. Park, Y.T. Kim, K.H. Park, Shape and Composition Control of Monodisperse Hybrid Pt-CoO Nanocrystals by Controlling the Reaction Kinetics with Additives, Sci. Rep. 7 (2017) 3851.

[37] H. Zheng, K. Feng, Y. Shang, Z. Kang, X. Sun, J. Zhong, Cube-like CuCoO nanostructures on reduced graphene oxide for H_2 generation from ammonia

494 borane, Inorg. Chem. Front. 5 (2018) 1180-1187.
495 [38] L. Jian, H. Zhang, B. Liu, C. Pan, Y. Dong, G. Wang, J. Zhong, Y. Zheng, Y.
496 Zhu, Monodisperse Ni-clusters anchored on carbon nitride for efficient
497 photocatalytic hydrogen evolution, Chinese J. Catal. 43 (2022) 536-545.
498 [39] K. Feng, H. Zhang, J. Gao, J. Xu, Y. Dong, Z. Kang, J. Zhong, Single atoms or
499 not? The limitation of EXAFS, Appl. Phys. Lett. 116 (2020) 191903.
500 [40] C.Y. Peng, L. Kang, S. Cao, Y. Chen, Z.S. Lin, W.F. Fu, Nanostructured Ni_2P as
501 a Robust Catalyst for the Hydrolytic Dehydrogenation of Ammonia-Borane,
502 Angew. Chem. Int. Ed. 54 (2015) 15725-15729.
503 [41] J. Zhong, H. Zhang, X. Sun, S.T. Lee, Synchrotron soft X-ray absorption
504 spectroscopy study of carbon and silicon nanostructures for energy applications,
505 Adv. Mater. 26 (2014) 7786-7806.